micro

MDPI

Article

A Comparative Study Between Micro and Millimeter Impedance Sensor Designs for Type-2 Diabetes Detection

Santu Guin [1,*], Debjyoti Chowdhury [2] and Madhurima Chattopadhyay [2]

[1] Electronics and Instrumentation Engineering, Techno Main Salt Lake, Salt Lake, Sector-5, Kolkata 700091, West Bengal, India
[2] Applied Electronics and Instrumentation Engineering, Heritage Institute of Technology, Chowbaga Road, Kolkata 700107, West Bengal, India; debjyoti.chowdhury@heritageit.edu (D.C.); madhurima.chattopadhyay@heritageit.edu (M.C.)
* Correspondence: santuguin@gmail.com

Abstract: In recent years, various types of sensors have been developed at both millimeter (mm) and micrometer (µm) scales for numerous biomedical applications. Each design has its own advantages and limitations. This study compares the electrical characteristics and sensitivity of millimeter- and micrometer-scale sensors, emphasizing the superior performance of millimeter-scale designs for detecting type-2 diabetes. Elevated glucose levels in type-2 diabetes alter the complex permittivity of red blood cells (RBCs), affecting their rheological and electrical properties, such as viscosity, volume, relative permittivity, dielectric loss, and AC conductivity. These alterations may manifest as a unique bio-impedance signature, offering a diagnostic topology for diabetes. In view of this, various concentrations (ranging from 10% to 100%) of 400 µL of normal and diabetic RBCs suspended in phosphate-buffered saline (PBS) solution are examined to record the changes in bio-impedance signatures across a spectrum of frequencies, ranging from 1 MHz to 10 MHz. In this study, simulations are performed using the finite element method (FEM) with COMSOL Multiphysics® to analyze the electrical behavior of the sensors at both millimeter (mm) and micrometer (µm) scales. These simulations provide valuable insights into the performance parameters of the sensors, aiding in the selection of the most effective design by using this topology.

Keywords: type-2 diabetes; complex permittivity; red blood cells (RBCs); bio-impedance signature; rheological characteristics; electrical behavior; finite element method (FEM)

check for updates

Academic Editor: Zhou Li

Received: 12 November 2024
Revised: 21 January 2025
Accepted: 27 January 2025
Published: 1 February 2025

Citation: Guin, S.; Chowdhury, D.; Chattopadhyay, M. A Comparative Study Between Micro and Millimeter Impedance Sensor Designs for Type-2 Diabetes Detection. *Micro* **2025**, *5*, 7. https://doi.org/10.3390/micro5010007

Copyright: © 2025 by the authors. Licensee MDPI, Basel, Switzerland. This article is an open access article distributed under the terms and conditions of the Creative Commons Attribution (CC BY) license (https://creativecommons.org/licenses/by/4.0/).

1. Introduction

Blood glucose levels are crucial for managing diabetes, a growing health concern globally. Governments, health departments, and medical professionals worldwide are increasingly focused on addressing this issue. As a key health indicator, blood glucose values play a significant role in clinical medicine [1,2]. Over 500 million people worldwide suffer from diabetes mellitus, also known as diabetes, which is a complicated and worrisome health disease [3]. This number is anticipated to expand significantly by 46 percent to 643 million by 2030 and 783 million by 2045, according to forecasts by the International Diabetes Federation (IDF) [4]. This illness results from either the body producing too little insulin or using the insulin it does make poorly. More than 90% of cases of diabetes worldwide are type 2, which is the most common type [5].

Ideal post-prandial (after eating) blood glucose levels should be below 180 mg/dL [6]. Diabetes is diagnosed based on elevated post-meal blood glucose levels. Normal blood

glucose levels range between 70 and 125 mg/dL. Hypoglycemia occurs when blood glucose is below 60 mg/dL (3.3 mmol/L), while hyperglycemia occurs when blood glucose is above 140 mg/dL (7.8 mmol/L) [7,8]. Several serious health hazards are associated with elevated glucose levels, including heart disease, stroke, renal failure, lower limb amputation, and visual impairment [9].

Blood glucose testing is typically carried out with venous samples in pathology labs [10] or home-based monitoring techniques [11–13]. Home-based monitoring uses a finger-pricking test and measurement can be carried out by the enzymatic–amperometric method [14]. Regular finger-pricking and the constant need to purchase test strips deter many patients from checking their glucose levels regularly due to pain, discomfort, and cost [15]. The two procedures that are recommended for lab-based blood glucose measurement are hexokinase and enzymatic–amperometric [16]. Using common spectrophotometric methods, glucose can be measured via the hexokinase method [17], while the enzymatic–amperometric is an alternative method of measuring glucose concentration using electrochemical sensors, which react blood samples with reagents and glucose oxidase [1]. The hexokinase techniques can be carried out using equipment such as Abbott AEROSET®(Chicago, IL, USA), Abbott ARCHITECT c8000®(Chicago, IL, USA), Hitachi 917 (Tokyo, Japan), and Cobas C701/C702 (Basel, Switzerland) [18]. Conversely, the enzymatic equipment includes the Biosen C-Line/S-Line (Cardiff, UK), YSI 2700 (Yellow Springs, OH, USA), and YSI 2950D (Yellow Springs, OH, USA) [19–22]. Laboratory methods are inherently disadvantageous due to the need for skilled personnel, which raises costs, and the longer wait times for detection, necessitating immediate completion to avoid a gradual decrease in concentration. Furthermore, challenges arise, particularly in cases of unstable hemodynamics, due to recent research demonstrating disparities in accuracy among some laboratory equipment, particularly in blood gas analysis and hypoglycemia detection [23].

Recent progress in sensor technology and nanomaterials offers exciting possibilities for miniaturized and highly accurate biosensors [16,24]. Capacitive sensors, which are widely used in this context, utilize either a parallel plate (PP) configuration or an interdigitated electrode (IDE) design to detect changes in capacitance and impedance [25]. These sensors are highly sought after for their flexible design, superior performance, and well-established fabrication process [26]. Advances in sensor miniaturization have enabled the development of millimeter (mm)-scale designs, which offer practical benefits such as enhanced sensitivity and adaptability for biomedical applications, including non-invasive diabetes detection [13,26,27]. In the year 2013, Zoric et al. [28] investigated the application of mm-size IDE sensors based on low-temperature co-fired ceramic (LTCC) material for environmental monitoring. By adding a dielectric material that electrically reacts to the desired property, the suggested detecting layer for this sensor can be adjusted to detect other gasses. Later in 2022, Li et al. [29] conducted simulation studies on mm-scale IDE-based impedance sensors to investigate impedance changes in water solutions with varying conductivities, revealing a significant response in electric-field density. The following year, Ullah et al. [26] proposed an extremely adaptable, sensitive, eco-friendly, economical, and highly efficient humidity sensor based on an IDE at mm scale. In the same year, Aldhaheri et al. [27] developed a flat, compact, and extremely sensitive arrow-shaped mm-scale microwave antenna sensor for measuring glucose concentration in blood. Additionally, they evaluated the Q-factor and sensitivity to assess the performance of the said sensor. Taking into account frequency-dependent dielectric characteristics, Ribas et al. [13] suggested a mm-scale planar electromagnetic resonator sensor to test blood glucose from the fingertip. On the other hand, an electrochemical microelectrode sensor for determining pH and concentrations of biomolecules was developed by Muaz et al. [30] in 2014. The different pH levels were used to measure the capacitance and current of the said sensor.

The following year, MacKay et al. [31] used simulations on an IDE-based impedance sensor to study the impact of ions in a solution over time, focusing on developing electric screening layers above the electrodes and examining the electric fields between the electrode digits. Later on, Hatada et al. [32] developed a highly sensitive, disposable amperometric strip for measuring glycated albumin (GA), a key glycemic control marker for diabetes mellitus, using a micro IDE as the electrode platform. In the year 2023, Nguyen et al. [33,34] developed a micro-IDE biosensor using ZnS-doped and Mn-capped chitosan nanomaterials for electrochemical and optical glucose-sensing applications, respectively. In recent years, by employing IDE impedimetric biosensors, Jiang et al. [35] examined the concentration levels of SARS-CoV-2 monoclonal antibodies (mAb).

The existing literature suggests that both mm-scale and µm-scale designs have the potential for blood glucose sensing [13,27,32–34,36–40]. IDE sensors offer a promising alternative, leveraging the bio-impedance signatures of blood glucose levels based on its dielectric properties [25,26,41–51]. However, the comparative performance of mm- and µm-scale IDE sensors in glucose detection remains unexplored. This study addresses this gap by systematically evaluating IDE sensors at these two scales, focusing on their sensitivity and bio-impedance response across a 1 MHz to 10 MHz frequency spectrum, aiming to develop non-invasive, cost-effective, and clinically adaptable glucose monitoring solutions. A more detailed comparison of the proposed methods to existing glucose-monitoring technologies is depicted in Table 1.

Table 1. A comparison of glucose-monitoring technologies with the proposed work.

Sl. No.	Technology	Description	Comparison with Our Work
1	Finger-Prick Test [14,15]	Uses test strips and pricking, causing discomfort and recurring costs.	Our method eliminates the need for pricking and consumables, providing a painless and cost-effective solution.
2	Hexokinase Method [16,17]	Lab-based technique requiring skilled personnel and high costs.	Our sensors are portable, suitable for point-of-care use, and reduce dependency on lab facilities.
3	Enzymatic–Amperometric Sensors[1,12]	Reagent-based electrochemical sensing.	Our reagent-free design offers a broader sensitivity range and reduced operational complexity
4	Capacitive Sensors [25,26]	Measures capacitance, typically used in non-biomedical fields.	We adapt this technology for bio-impedance-based glucose sensing, optimized for both mm and µm scales.
5	Microwave Antenna Sensors [13,27]	Highly sensitive but complex and less clinically adopted.	Our IDE sensors achieve comparable sensitivity while being simpler and more adaptable to clinical use.

The main contributions of this work are:

1. Demonstrate the methodology for blood glucose detection based on the bio-impedance signature study.
2. Establish a performance comparison between mm and µm structured IDE design for bio-impedance signature-based blood glucose detection.

3. Analysis of sensitivity for both types of sensors (mm and µm) across the entire range of concentrations within the 1 MHz to 10 MHz frequency spectrum.

2. Materials and Methods

2.1. Bio-Impedance Measurement

When a suspension of cells in a phosphate-buffered saline solution (PBS) is exposed to an electric potential, it allows for the measurement of bio-impedance at different frequencies [36,52,53]. The resulting complex impedance reveals the cells' electrical characteristics, influenced by the applied voltage and frequency, affecting the dielectric properties of cells like red blood cells (RBCs) [53,54]. Maxwell's mixing theory, as stated in Equation (1), explains the equivalent complex dielectric permittivity, helping to understand the electrical behavior of the cell suspension in response to the applied potential and frequency changes [55–57].

$$\varepsilon_{\text{mix}} = \varepsilon_m \left(\frac{1 + 2\phi f_{\text{CM}}}{1 - \phi f_{\text{CM}}}\right) \tag{1}$$

This Equation (1) explains how the complex permittivity of a cell suspension (ε_{mix}) is affected by the suspending medium's permittivity (ε_m), the cell volume ratio (ϕ), and the complex Clausius–Mossotti factor (f_{CM}), illustrating the impact of cell volume fraction and their interaction with the electric field on the suspension's electrical properties [52,55]. The volume fraction (ϕ) can be computed using Equation (2) and a single-shell ellipsoid model, which provides a straightforward but informative method of comprehending the distribution and electrical behavior of the cells in suspension [55].

$$\phi = \frac{200 \times 10^6 \times \frac{4}{3}\pi R^3}{400 \times 10^{-6} \times 10^{-3}} \tag{2}$$

Here, 200 million cells are analyzed in 400 µL of phosphate-buffered saline (PBS) solution; the resulting values of ϕ are 0.133 and 0.062 for normal and diabetic blood, respectively. The Clausius—Mossotti factor is defined by Equation (3):

$$f_{\text{CM}} = \frac{\varepsilon_{\text{cell}} - \varepsilon_m}{\varepsilon_{\text{cell}} + 2\varepsilon_m} \tag{3}$$

where Equation (4) gives the complex permittivity for the cell, which is represented by $\varepsilon_{\text{cell}}$ [36,52].

$$\varepsilon_{\text{cell}} = \varepsilon_{\text{mem}} \left(\frac{\rho^3 + 2\frac{\varepsilon_i - \varepsilon_m}{\varepsilon_i + 2\varepsilon_m}}{\rho^3 - \frac{\varepsilon_i - \varepsilon_m}{\varepsilon_i + 2\varepsilon_m}}\right) \tag{4}$$

and

$$\rho = \frac{R}{R - d} \tag{5}$$

where R is the cell radius, d is the membrane thickness, and ε_i and ε_{mem} are the permittivity of the cytoplasm and the cell membrane, respectively.

Using Table 2 and the values from Equations (4) and (5), we determined the permittivity values ($\varepsilon_{\text{cell}}$) for normal and diabetic blood to be 3.441 F/m and 4.431 F/m, respectively, based on the suspending medium's permittivity (ε_m) and conductivity (σ_m) [52]. The complex Clausius–Mossotti factor (f_{CM}) values for normal and diabetic red blood cells are −0.46 and −0.45, respectively, which are used in Equation (1) to calculate the complex permittivity (ε_{mix}) values for the blood cells in PBS mixture, yielding 66.16 and 73.48, respectively [55]. To evaluate the mixture's conductivity, we examine the variables related to electrical conductivity in Equations (1) and (3), leading to Equation (6), which provides

an expression for the total conductivity (σ_{mix}) and helps understand the influence of the mixture's constituents on its electrical properties [55].

$$\begin{aligned}\sigma_{\text{mix}} &= \sigma_m \frac{1 + 2\phi\left(\frac{\sigma_i - \sigma_m}{\sigma_i + 2\sigma_m}\right)}{1 - \phi\left(\frac{\sigma_i - \sigma_m}{\sigma_i} + 2\sigma_m\right)} \\ &= \sigma_m \left[1 + 3\phi \frac{\sigma_i - \sigma_m}{(1-\phi)\sigma_i + (2+\phi)\sigma_m}\right]\end{aligned} \tag{6}$$

When the volume fraction (ϕ) is low ($\ll$1), Maxwell's approximation [58] states that Equation (6) can be approximately

$$\sigma_{\text{mix}} \simeq \sigma_m \left(1 + 3\phi \frac{\sigma_i - \sigma_m}{\sigma_i + 2\sigma_m}\right) \tag{7}$$

This Equation (7) can be utilized to calculate the mixture conductivity for normal and diabetic red blood cells as 0.63 and 0.68 S/m, respectively. Due to the significant variance in (ε_{mix}) and relatively minor change in (σ_{mix}) between normal and diabetic RBCs, conductivity is not used as a criterion for identifying diabetes in this study. Table 3 summarizes the parameter changes for both normal and diabetic RBCs [53].

Table 2. Physical and electrical parameters of normal and diabetic RBC [52,54,59,60].

Sl. No.	Parameters	Normal RBC	Diabetic RBC
1	Cytoplasmic radius (R)	4 µm	3.1 µm
2	Cytoplasm permittivity (ε_i)	62	75.64
3	Cytoplasm conductivity (σ_i)	0.32 S/m	0.457 S/m
4	Membrane thickness (d)	40 nm	2.68 µm
5	Membrane permittivity (ε_{mem})	4.44	5.41

Table 3. Changes in parameters for normal and diabetic RBC.

Sl. No.	RBC Type	ϕ	f_{CM}	ε_{mix}	σ_{mix}
1	Normal RBC	0.133	−0.46	66.16	0.63
2	Diabetic RBC	0.062	−0.45	73.48	0.68

2.2. Capacitive Sensor Design in the Simulator

The IDE capacitive sensor has been chosen for simulation using COMSOL Multiphysics® to simplify the design process for measuring bio-impedance data through finite element analysis [55]. This study focuses on a millimeter-scale sensor design featuring a 15 mm × 0.1 mm electrode area on a 0.1 mm thick Silicon-on-Insulator (SoI) wafer with 2.5 mm spacing between electrode pairs, comparing its performance with a micrometer-scale design for context [53]. The essential design parameters are summarized in Table 4. COMSOL Multiphysics, based on the finite element method, solves partial differential equations to simulate complex physical phenomena. This study uses COMSOL's AC/DC module to model and analyze IDE-based sensors in a conducting medium, focusing on electric-field distribution and impedance calculation. The model setup involves material selection, applying voltage (high and ground), meshing, and defining frequency-domain parameters. The electrical conduction current density is calculated using:

$$J = (\sigma + j\omega\varepsilon_0\varepsilon_r)E + J_e \tag{8}$$

where σ is the conductivity, ω is the angular frequency, ε_0 is the vacuum permittivity, ε_r is the relative permittivity, E is the electric field, and J_e is the externally generated current density.

Table 4. The design parameters of IDE used in the simulator [53].

Serial No.	Parameters	Values	
		in mm Dimension	in µm Dimension
1	Material of IDE	Silicon	Silicon
2	Number of IDE	6	6
3	Area of IDE	15 mm × 0.1 mm	116 µm × 50 µm
4	Distance between electrode pairs	2.5 mm	5 µm

In this proposed methodology, the mm-scale electrode layout is shown in Figure 1, with Figure 1a displaying a rack distance of 20 mm for the interdigitated electrodes (IDEs) and a 2.5 mm gap between each pair, while Figure 1b shows the electrode depth as 0.1 mm on a 0.1 mm thick silicon substrate. The µm-scale electrode configuration is displayed in Figure 2, with Figure 2a showing a 126 µm distance between IDE racks and a 5 µm gap between each pair, and Figure 2b showing the electrode depth as 50 µm. There are 40 capacitive elements in parallel, and the complex bio-impedance (Z_{mix}) measured by both configurations at a fixed frequency (f) is given by Equation (9) [53,55]:

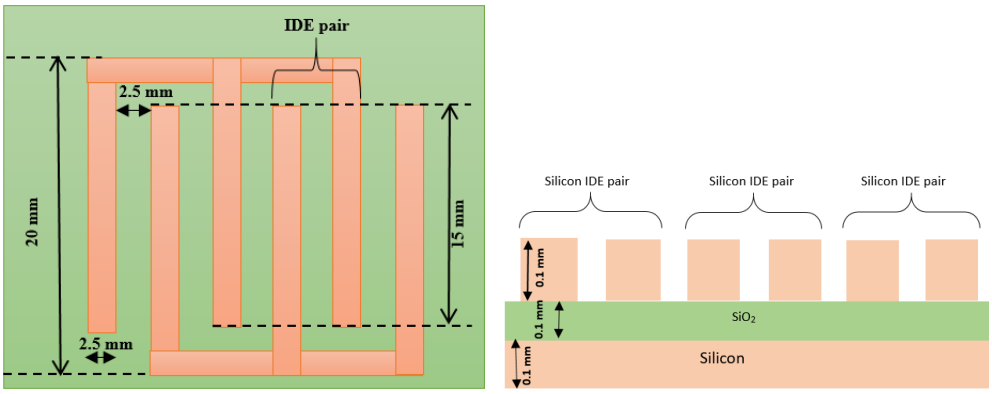

(**a**) middle view. (**b**) cross section view.

Figure 1. Electrode layout with millimeter (mm) dimension with (**a**) top view; (**b**) cross-section view.

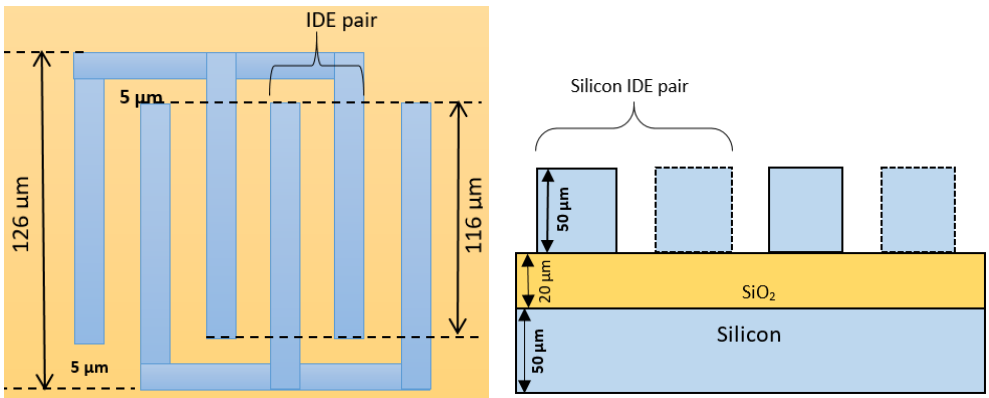

(**a**) top view. (**b**) cross section view.

Figure 2. Electrode layout with micrometer (µm) dimension with (**a**) top view; (**b**) cross-section view [53,55].

$$Z_{\text{mix}} = \frac{1}{2\pi f[40(\varepsilon_o \varepsilon_{\text{mix}} G)]} \tag{9}$$

where G is the geometric constant (ratio of electrode area to the gap between pairs) equal to 0.6 mm and 1160 µm for the configurations in Figures 1a and 2a, respectively. Both designs are simulated in COMSOL® using the AC/DC module to solve Maxwell's equations, enabling the calculation of frequency-dependent impedance values [52,55]. A graphic representation of the impact of variations in cell count on the complex permittivity of the cell–medium interaction is provided in Figure 3, which also displays different ε_{mix} values for healthy and diabetic blood cells in the PBS mixture in Table 5.

Table 5. Changes in cell–medium complex permittivity with varying numbers of cells [53].

Sl. No.	Number of Cells (Million)	ε_{mix} for Normal RBC	ε_{mix} for Diabetic RBC
1	100	72.92	76.67
2	150	69.44	75.05
3	200	65.12	73.44
4	250	62.87	71.86

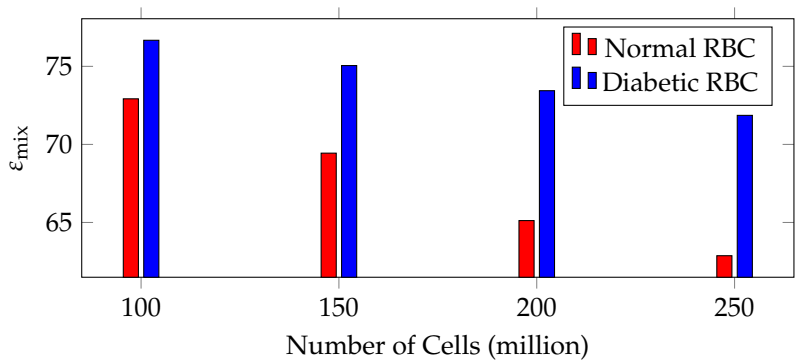

Figure 3. Variation in the permittivity of the cell–medium with an increasing number of cells [53].

2.3. Sensor Properties

2.3.1. Cell Factor Calculation

Equation (10) relates the resistance (R_{sol}) and capacitance (C_{sol}) of the ionic solution to electrolyte conductivity and permittivity through a cell factor K_{cell} [53,55], while Equation (11) determines this factor using sensor geometries as input.

$$R_{\text{sol}} = \frac{K_{\text{cell}}}{\sigma_{\text{sol}}}; \quad C_{\text{sol}} = \frac{\varepsilon_0 \varepsilon_{\text{r, sol}}}{K_{\text{cell}}} \tag{10}$$

$$K_{\text{cell}} = \frac{2}{L(N-1)} \frac{K(k)}{K\left(\sqrt{1-k^2}\right)} \tag{11}$$

where $\varepsilon_{\text{r, sol}}$ is the electrolyte's relative permittivity, and σ_{sol} denotes the electrolyte conductivity (measured in S/m); N is the number of digits (of which there are 40), and L is the digit length (µm). The metalization ratio, denoted as $\alpha = W/(S+W)$, where W is the digit width, and S is the spacing between two digits, is used to calculate the cell factor (K_{cell}) through Equation (12) involving the incomplete integral of the first module $K(k)$,

yielding K_{cell} values of 2.82 m^{-1} and 365.09 m^{-1} for electrodes with mm and µm-scale dimensions, respectively.

$$K(k) = \int_0^1 \frac{1}{\sqrt{(1-t^2)(1-k^2t^2)}}dt \quad \text{with } k = \cos\left(\frac{\pi}{2}\frac{W}{S+W}\right) \tag{12}$$

2.3.2. Double-Layer Capacitance

When a voltage is applied, charge segregation at the electrode–electrolyte interface creates double-layer capacitance, which significantly impacts the system's overall impedance [53]. The capacitance at the interface for each positive electrode ($C_{int,p}$) and each negative electrode ($C_{int,n}$) is determined using Equation (13) [55].

$$C_{int,p} = C_{int,n} = LWC_0, \tag{13}$$

With an equal number of positive and negative electrodes $(N/2)$, the overall capacitance for each type of electrode is given by the Equation (14) [55].

$$\frac{N}{2}C_{int,p} = \frac{N}{2}C_{int,n} \tag{14}$$

The total capacitance, or double-layer capacitance (C_{DL}), is calculated using Equation (15).

$$C_{DL} = \frac{N}{4}LWC_0 \tag{15}$$

For both mm and µm scale designs with 40 electrodes (N), the values of C_{DL} are 105 pF/m^{-2} and 4.06 pF/m^{-2}, respectively.

2.3.3. Double Layer Impedance

The double-layer impedance (Z_{DL}) characterizes interface phenomena when polarized electrodes interface with an electrolyte, involving two parallel layers of charge on a localized section (mm or µm) of the electrode surface [53]. These phenomena challenge low-frequency measurements and are crucial for overall modeling. Despite their intricacy, Z_{DL} is calculated within the 1 MHz to 10 MHz range using Equation (16):

$$Z_{DL} = \frac{1}{j\omega C_{DL}} \tag{16}$$

where j is the imaginary unit and ω is the angular frequency in rad/s. For both mm and µm dimensions with 40 electrodes, the absolute Z_{DL} values (in MΩ) are summarized in Table 6, with surface capacitance (C_0) values of 2.8×10^{-7} F/m^{-1} and 7×10^{-4} F/m^{-1}, respectively.

Table 6. Parameters for the double-layer impedance of IDE.

Sl. No.	Dimension of Electrodes	K_{cell} (m^{-1})	C_{DL} (pF/m^2)	Z_{DL} (MΩ)									
				1 MHz	2 MHz	3 MHz	4 MHz	5 MHz	6 MHz	7 MHz	8 MHz	9 MHz	10 MHz
1	mm	2.82	105	1.51	0.75	0.50	0.37	0.30	0.25	0.21	0.18	0.16	0.15
2	µm	365.09	4.06	39.2	19.61	13.07	9.80	7.84	6.53	5.60	4.90	4.35	3.92

3. Results

3.1. Average Impedance

Our study highlights significant variations in bio-impedance data due to changes in the electrical properties of the PBS solution used for measurements involving 200 million cells. These electrical property variations stem from the difference between healthy and diabetic blood cells. The Z_{mix} value across the frequency range of 1 MHz to 10 MHz plays a key role in this phenomenon. As suggested by previous research [52,53], we calculated and tabulated the Z_{mix} values for two design configurations (one with mm and another with µm dimensions) in Tables 7 and 8. Figures 4 and 5 visually represent the surface-charge density of interdigitated electrodes (IDEs) interacting with the medium within a COMSOL® simulation environment. These figures utilize electrodes with mm dimensions. Similarly, Figure 6 depicts the surface charge density of IDEs interacting with the medium in COMSOL® but with µm-sized electrodes.

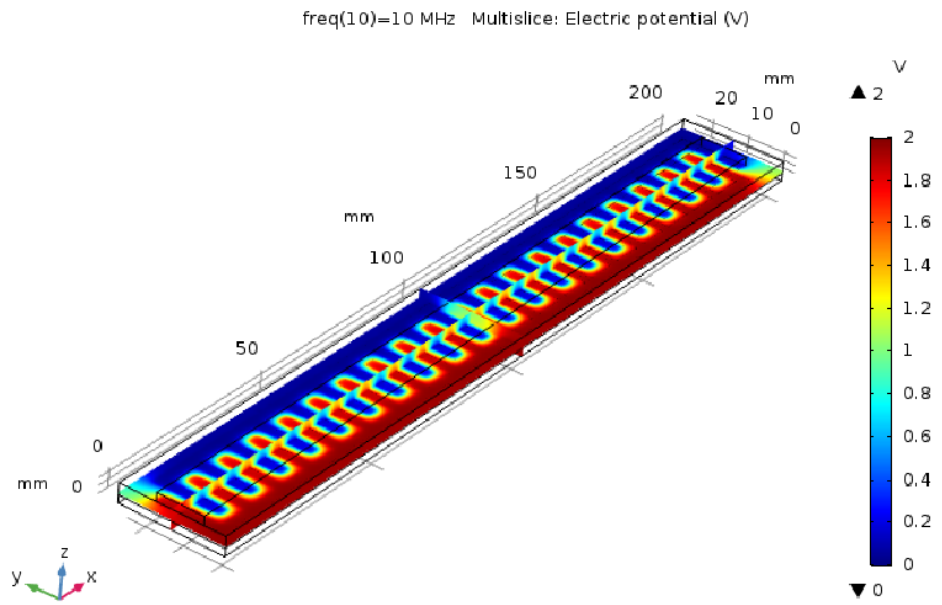

Figure 4. Surface-charge density in diabetic RBC with mm electrodes.

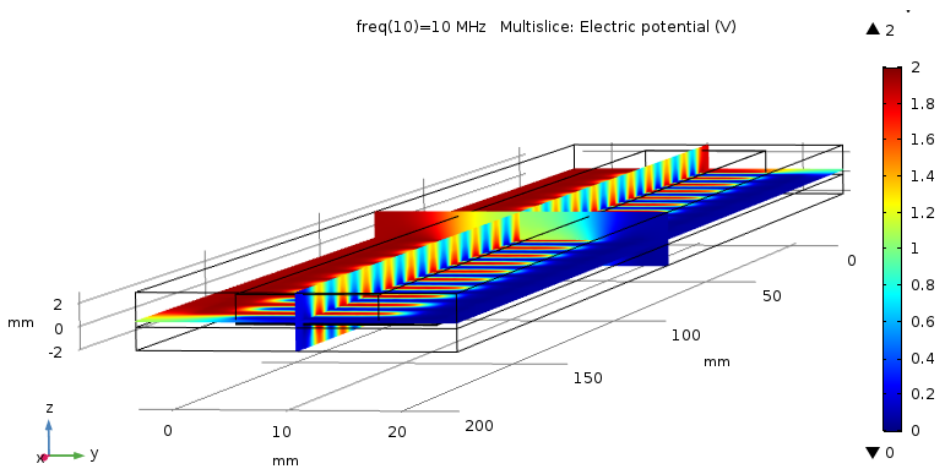

Figure 5. Surface-charge density of diabetic RBC with mm electrodes (Y-Z direction).

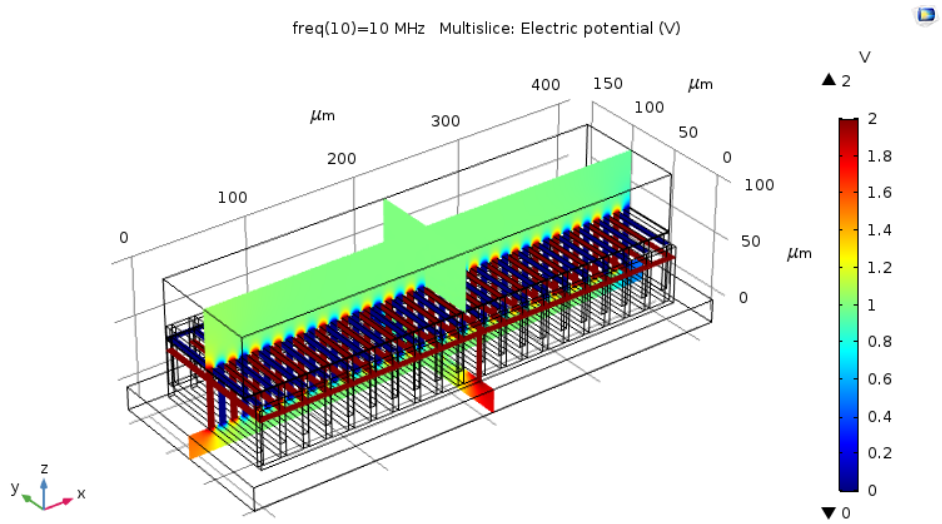

Figure 6. Surface-charge density of diabetic RBC with µm electrodes.

As evident from Figure 7, µm-sized IDEs exhibit a superior response compared to mm-sized ones.

Table 7. Comparison of electrical properties of normal and diabetic RBC in PBS mixture using 40 electrodes in mm dimension.

(a) Variation in electrical properties of normal RBC in PBS mixture over different concentrations using 40 capacitive elements in mm dimension

Sl. No.	Concentration (%)	Volume Fraction (ϕ)	Z_{mix} (kΩ)										Average Z_{mix} (kΩ)
			1 MHz	2 MHz	3 MHz	4 MHz	5 MHz	6 MHz	7 MHz	8 MHz	9 MHz	10 MHz	
1	100	0.133	11.326	5.633	3.775	2.831	2.265	1.887	1.618	1.415	1.258	1.132	3.314
2	90	0.120	11.111	5.555	3.703	2.777	2.222	1.851	1.587	1.388	1.234	1.111	3.254
3	80	0.107	10.901	5.450	3.633	2.725	2.180	1.816	1.557	1.362	1.211	1.090	3.193
4	70	0.093	10.682	5.341	3.560	2.670	2.136	1.780	1.526	1.335	1.186	1.068	3.128
5	60	0.080	10.483	5.241	3.494	2.620	2.096	1.747	1.497	1.310	1.164	1.048	3.070
6	50	0.066	10.276	5.138	3.425	2.569	2.055	1.712	1.468	1.284	1.141	1.027	3.010
7	40	0.053	10.088	5.044	3.362	2.522	2.017	1.681	1.441	1.261	1.120	1.008	2.954
8	30	0.040	9.904	4.952	3.301	2.476	1.980	1.650	1.414	1.238	1.100	0.990	2.901
9	20	0.026	9.711	4.855	3.237	2.427	1.942	1.618	1.387	1.213	1.079	0.971	2.844
10	10	0.013	9.537	4.768	3.179	2.384	1.907	1.589	1.362	1.192	1.059	0.953	2.793

(b) Variation in electrical properties of diabetic RBC in PBS mixture over different concentrations using 40 capacitive elements in mm dimension

Sl. No.	Concentration (%)	Volume Fraction (ϕ)	Z_{mix} (kΩ)										Average Z_{mix} (kΩ)
			1 MHz	2 MHz	3 MHz	4 MHz	5 MHz	6 MHz	7 MHz	8 MHz	9 MHz	10 MHz	
1	100	0.062	10.198	5.099	3.399	2.549	2.039	1.699	1.456	1.274	1.133	1.019	2.987
2	90	0.056	10.112	5.056	3.370	2.528	2.022	1.685	1.444	1.264	1.123	1.011	2.962
3	80	0.049	10.015	5.077	3.338	2.503	2.003	1.669	1.430	1.251	1.112	1.001	2.940
4	70	0.043	9.933	4.966	3.311	2.483	1.986	1.655	1.419	1.241	1.103	0.993	2.909
5	60	0.037	9.852	4.926	3.284	2.463	1.970	1.642	1.407	1.231	1.094	0.985	2.885
6	50	0.031	9.771	4.885	3.257	2.442	1.954	1.628	1.395	1.221	1.085	0.977	2.862
7	40	0.024	9.677	4.838	3.225	2.419	1.935	1.612	1.382	1.209	1.075	0.967	2.834
8	30	0.018	9.598	4.799	3.199	2.399	1.919	1.599	1.371	1.199	1.066	0.959	2.811
9	20	0.012	9.520	4.760	3.173	2.380	1.904	1.586	1.360	1.190	1.057	0.952	2.788
10	10	0.006	9.443	4.721	3.147	2.360	1.888	1.573	1.349	1.180	1.049	0.944	2.765

Table 8. Comparison of electrical properties of normal and diabetic RBC in PBS mixture using 40 electrodes in µm dimension.

(a) Variation in electrical properties of normal RBC in PBS mixture over different concentrations using 40 capacitive elements in µm dimension

Sl. No.	Concentration (%)	Volume Fraction (ϕ)	Z_{mix} (kΩ)										Average Z_{mix} (kΩ)
			1 MHz	2 MHz	3 MHz	4 MHz	5 MHz	6 MHz	7 MHz	8 MHz	9 MHz	10 MHz	
1	100	0.133	5.858	2.929	1.952	1.464	1.171	0.976	0.836	0.732	0.650	0.585	1.715
2	90	0.120	5.747	2.873	1.915	1.436	1.149	0.957	0.821	0.718	0.638	0.574	1.683
3	80	0.107	5.638	2.819	1.879	1.409	1.127	0.939	0.805	0.704	0.626	0.563	1.651
4	70	0.093	5.525	2.762	1.841	1.381	1.105	0.920	0.789	0.690	0.613	0.552	1.618
5	60	0.080	5.422	2.711	1.807	1.355	1.084	0.903	0.774	0.677	0.602	0.542	1.588
6	50	0.066	5.315	2.657	1.771	1.328	1.063	0.885	0.759	0.664	0.590	0.531	1.556
7	40	0.053	5.218	2.609	1.739	1.304	1.043	0.869	0.745	0.652	0.579	0.521	1.528
8	30	0.040	5.122	2.561	1.707	1.280	1.024	0.853	0.731	0.640	0.569	0.512	1.500
9	20	0.026	5.023	2.511	1.674	1.255	1.004	0.837	0.717	0.627	0.558	0.502	1.471
10	10	0.013	4.933	2.466	1.664	1.233	0.986	0.822	0.704	0.616	0.548	0.493	1.447

(b) Variation in electrical properties of diabetic RBC in PBS mixture over different concentrations using 40 capacitive elements in µm dimension

Sl. No.	Concentration (%)	Volume Fraction (ϕ)	Z_{mix} (kΩ)										Average Z_{mix} (kΩ)
			1 MHz	2 MHz	3 MHz	4 MHz	5 MHz	6 MHz	7 MHz	8 MHz	9 MHz	10 MHz	
1	100	0.062	5.274	2.637	1.758	1.318	1.054	0.879	0.753	0.659	0.586	0.527	1.545
2	90	0.056	5.230	2.615	1.743	1.307	1.046	0.871	0.747	0.653	0.581	0.523	1.532
3	80	0.049	5.180	2.590	1.726	1.295	1.036	0.863	0.740	0.647	0.575	0.518	1.517
4	70	0.043	5.137	2.568	1.712	1.284	1.027	0.856	0.733	0.642	0.570	0.513	1.504
5	60	0.037	5.095	2.547	1.698	1.273	1.019	0.849	0.727	0.636	0.566	0.509	1.492
6	50	0.031	5.054	2.527	1.684	1.263	1.010	0.842	0.722	0.631	0.561	0.505	1.480
7	40	0.024	5.005	2.502	1.668	1.251	1.001	0.834	0.715	0.625	0.556	0.500	1.466
8	30	0.018	4.964	2.482	1.654	1.241	0.992	0.827	0.709	0.620	0.551	0.496	1.454
9	20	0.012	4.924	2.462	1.641	1.231	0.984	0.820	0.703	0.615	0.547	0.492	1.442
10	10	0.006	4.884	2.442	1.628	1.221	0.976	0.814	0.697	0.610	0.542	0.488	1.430

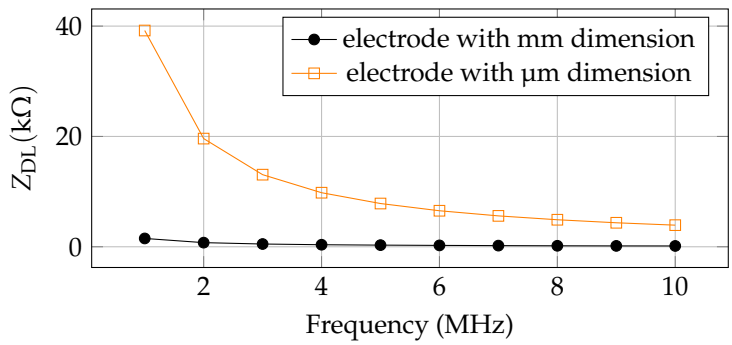

Figure 7. Variation of the double-layer impedance of IDE within 1 MHz–10 MHz using electrodes with mm dimension and µm dimension.

Figures 8 and 9 depict the variation in average complex impedance (Z_{mix}) across the entire concentration range within a frequency range of 1–10 MHz for 40 electrodes with both mm and µm dimensions.

These data are obtained by analyzing increasing RBC densities (both healthy and diseased) in a PBS solution. The average Z_{mix} is calculated to provide a comprehensive understanding of the overall impedance variation within the test frequency range. While these averages offer a general idea of the impedance variations (shown in Figures 8 and 9), a more detailed picture is achieved by examining these figures alongside the average Z_{mix} values presented in Tables 7 and 8. This combined analysis allows us to observe the impedance characteristics of healthy and diseased RBCs at various frequencies across the entire concentration range. The analysis considers factors like the number of electrodes

(N = 40) and electrode length (L = 15 mm in mm scale and L = 116 µm in µm configuration). Figures 8 and 9 highlight that millimeter-scale sensors consistently exhibit higher average Z_{mix} values for diabetic RBCs (2.987 kΩ at 100%) compared to normal RBCs (3.314 kΩ at 100%), showcasing their enhanced sensitivity. For mm-sized electrodes, the average Z_{mix} of normal RBCs increases from 2.793 kΩ at 10% to 3.314 kΩ at 100%, while diabetic RBCs show a similar trend, with 2.765 kΩ at 10% and 2.987 kΩ at 100%. Although µm-sized electrodes were included for comparison, their lower sensitivity (e.g., 1.715 kΩ for normal RBCs at 100%) highlights the superior performance of mm-sized electrodes for detecting average Z_{mix} variations. These Figures 10 and 11 illustrate the standard deviation (SD) of Z_{mix} (kΩ) for normal and diabetic RBCs across the entire concentration range at a 1–10 MHz frequency range, using both mm and µm-sized electrodes. These figures visually represent the disparity in the bio-impedance signatures of healthy and diabetic cells. The standard deviation for normal RBCs using mm-sized electrodes is 0.57 and 0.05 at 1 MHz and 10 MHz, respectively. Similarly, for diabetic RBCs, the values are 0.24 and 0.02 at 1 MHz and 10 MHz, respectively. For µm-sized electrodes (Figure 11), the standard deviation for normal RBCs is 0.29 and 0.02 at 1 MHz and 10 MHz, respectively, while for diabetic RBCs it is 0.12 and 0.01. A larger standard deviation at 1 MHz signifies greater variability in the bio-impedance data, indicating that the values are more scattered around the mean. This suggests less consistent or more dispersed readings at lower frequencies. Conversely, a lower standard deviation at 10 MHz reflects a tighter clustering of bio-impedance values around the mean, implying a more stable and reliable measurement environment. This trend suggests that µm-sized electrodes potentially offer reduced noise or interference, leading to more reliable bio-impedance measurements at 10 MHz compared to 1 MHz.

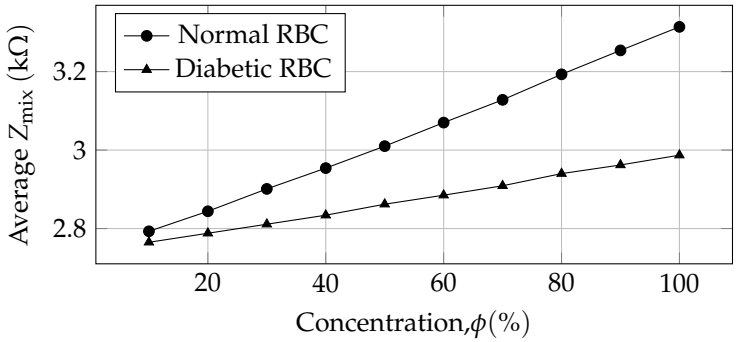

Figure 8. Variation in the average complex impedance (Z_{mix}) over the whole concentration range within 1–100 MHz frequency range for N = 40 (in mm dimension).

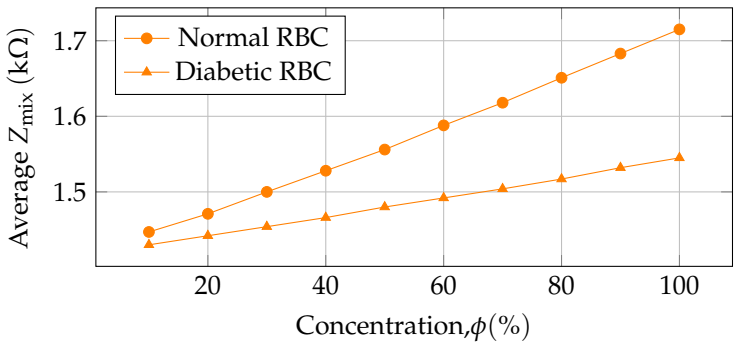

Figure 9. Variation in the average complex impedance (Z_{mix}) over the whole concentration range within 1–100 MHz frequency range for N = 40 (in µm dimension).

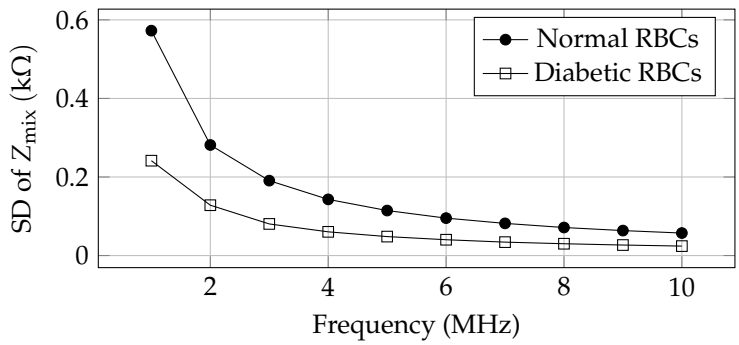

Figure 10. Standard deviation (SD) of Z_{mix} (kΩ) for normal and diabetic RBCs over the whole range of concentration by varying the frequency range within 1–10 MHz using electrodes with mm dimension.

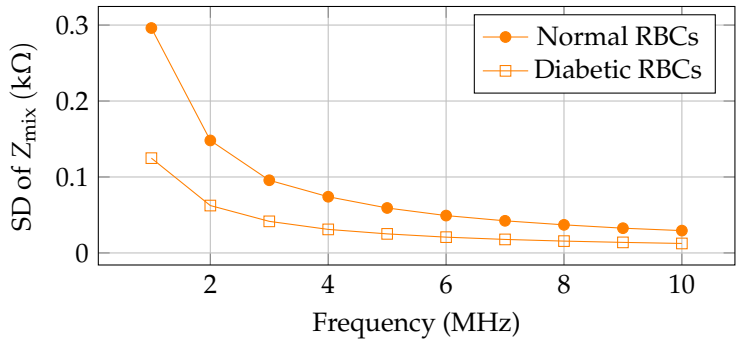

Figure 11. Standard deviation (SD) of Z_{mix} (kΩ) for normal and diabetic RBCs over the whole range of concentration by varying the frequency range 1–10 MHz using electrodes with µm dimension.

3.2. Sensitivity of the Designed Sensor

Sensitivity (SV) can be calculated by the ratio of Z_{mix} to ϕ using Equation (17). This equation is chosen so that the sensitivity estimate would be independent of the sensor's design characteristics.

$$SV = \frac{Z_{mix}}{\phi} \tag{17}$$

The average sensitivities of the mm-scale sensor for normal and diabetic RBCs are 65.198 and 136.643, respectively. For the µm scale sensor, the average sensitivities for normal and diabetic RBCs are 33.739 and 70.661, respectively, as shown in Table 9. This demonstrates the practical advantage of mm-scale designs in detecting diabetes-related impedance variations.

Table 9. Average sensitivity of normal and diabetic RBCs in different sensor designs.

RBC Type	Average Sensitivity (mm Design)	Average Sensitivity (µm Design)
Normal RBC	65.198	33.739
Diabetic RBC	136.643	70.661

4. Discussion

In diabetic individuals, healthy blood cells experience a decrease in cytoplasmic radius to approximately 3.1 µm, as depicted in Table 2. Using Equation (1), the complex permittivity of the RBC-PBS mixture within a 200 µm PBS solution is calculated, yielding values of 65.12 for healthy RBCs and 73.44 for diabetic RBCs, as shown in Table 3. This permittivity of the cell–medium complex is also influenced by the number of RBCs, as detailed in Table 5 and Figure 3. Furthermore, the bio-impedance signature of the cell–

medium mixture of both structures has been studied across a frequency range of 1–10 MHz for varying cell concentrations, as shown in Tables 7 and 8. Here, it has been observed that the cell-mixture impedance decreases with decreasing cell concentration for both mm and µm-designed electrodes. At 100% cell concentration, Figures 8 and 9 illustrate that the average bio-impedance of diabetic blood cells is lower compared to healthy ones. For mm-configured electrodes, the values are 2.987 kΩ and 3.314 kΩ for diabetic and healthy blood cells, respectively. Similarly, the values for µm-configured electrodes are 1.545 kΩ and 1.715 kΩ, respectively. The SD of the bio-impedance signatures for healthy and diabetic RBCs are visually represented in Figures 10 and 11, which highlight the difference in SD across the entire concentration range at various frequencies (1–10 MHz) for both mm and µm designed electrodes that indicate the bio-impedance measurements at 10 MHz frequency are more reliable or have less variability compared to the measurement at 1 MHz frequency.

The analysis confirms that mm-scale sensors exhibit superior sensitivity (9) and reliability compared to µm designs (Figures 1 and 2). The Z_{mix} is calculated within the frequency range of 1 MHz to 10 MHz mentioned in Tables 7 and 8. While both configurations differentiate diabetic RBCs from normal, the millimeter-scale sensor demonstrates higher practicality for diagnostic applications.

Similarly, it can be observed that both mm and µm designs have higher sensitivity (136.64 for mm and 70.66 for µm design) in detecting diabetic RBCs compared to non-diabetic ones. The higher sensitivity of the mm design can be attributed to the fact that the electrode spacing can accommodate a larger volume fraction of the cell PBS mixture compared to the µm design. Consequently, both sensor designs are more sensitive towards detecting diabetic RBCs than non-diabetic ones. This might lead to more false positives but fewer false negatives, which could be considered better for medical applications where missing a diagnosis (false negative) is more harmful than potential over-diagnosis (false positive).

5. Conclusions

This study explores a novel approach for identifying type-2 diabetes in human blood based on variations in the electrical properties of RBCs. To achieve the same, this work also introduces an IDE-based sensor design in both mm and µm scales. The sensitivity of the two structures is compared in this study to identify in which scale design the sensor is best suited for the said application. This study establishes the mm-scale sensor as the optimal choice for type-2 diabetes detection due to its superior sensitivity, reliability, and cost-effectiveness. µm designs are briefly addressed but are less practical for disposable and non-invasive applications, which are the focus of this work. This analysis suggests that both designed electrodes provide a good response for detecting type-2 diabetes, making either ideal for the application.

Author Contributions: Conceptualization, S.G. and M.C.; methodology, S.G. and D.C.; simulation, S.G.; validation, D.C. and M.C.; formal analysis, S.G.; investigation, S.G.; resources, M.C.; data curation, S.G.; writing—original draft preparation, S.G.; writing—review and editing, D.C. and M.C.; visualization, S.G.; supervision, D.C. and M.C. All authors have read and agreed to the published version of the manuscript.

Funding: This research received no external funding.

Institutional Review Board Statement: Not applicable.

Informed Consent Statement: Not applicable.

Data Availability Statement: The data presented in this study are available on request from the corresponding author.

Conflicts of Interest: The authors declare no conflicts of interest.

References

1. Wang, Z.; Liu, X.; Liu, Z.; Zhang, J.; Fang, T. A Continuous Blood Glucose Monitoring Front End IC Design with Large Input Range. In Proceedings of the 2023 8th International Conference On Integrated Circuits And Microsystems (ICICM), Nanjing, China, 20–23 October 2023; pp. 128–133.
2. Reza, M.; Song, H.; Lee, Y.; Asaduzzaman, M.; Cha, C.; Park, J. An Electrochemical Microneedle Biosensor with Wide Linear Range for Continuous Glucose Monitoring. In Proceedings of the 2023 IEEE SENSORS, Vienna, Austria, 29 October–1 November 2023; pp. 1–4.
3. Saeedi, P.; Petersohn, I.; Salpea, P.; Malanda, B.; Karuranga, S.; Unwin, N.; Colagiuri, S.; Guariguata, L.; Motala, A.; Ogurtsova, K. Others Global and regional diabetes prevalence estimates for 2019 and projections for 2030 and 2045: Results from the International Diabetes Federation Diabetes Atlas. *Diabetes Res. Clin. Pract.* **2019**, *157*, 107843. [CrossRef] [PubMed]
4. Udara, S.; De Alwis, A.; Silva, K.; Ananda, U.; Kahandawaarachchi, K. DiabiTech-Non-Invasive Blood Glucose Monitoring System. In Proceedings of the 2019 International Conference On Advancements In Computing (ICAC), Malabe, Sri Lanka, 5–7 December 2019; pp. 145–150.
5. Sun, H.; Saeedi, P.; Karuranga, S.; Pinkepank, M.; Ogurtsova, K.; Duncan, B.; Stein, C.; Basit, A.; Chan, J.; Mbanya, J. Others IDF Diabetes Atlas: Global, regional and country-level diabetes prevalence estimates for 2021 and projections for 2045. *Diabetes Res. Clin. Pract.* **2022**, *183*, 109119. [CrossRef] [PubMed]
6. Owida, H.; Al-Nabulsi, J.; Al Khatib, A. Equivalence of Fasting and Non-Fasting Blood Glucose Readings at the Palm and Fingertip Sites. In Proceedings of the 2022 13th International Conference On Information And Communication Systems (ICICS), Irbid, Jordan, 21–23 June 2022; pp. 411–415.
7. Association, A. Diagnosis and classification of diabetes mellitus. *Diabetes Care* **2014**, *37*, S81–S90. [CrossRef] [PubMed]
8. Baingane, A.; Slaughter, G. A glucose monitoring system with remote data access. *IEEE Trans. Nanobioscience* **2020**, *19*, 622–626. [CrossRef] [PubMed]
9. Kassem, A.; Hamad, M.; Harbieh, G.; El Moucary, C. A Non-Invasive Blood Glucose Monitoring Device. In Proceedings of the 2020 IEEE 5th Middle East And Africa Conference On Biomedical Engineering (MECBME), Amman, Jordan, 27–29 October 2020; pp. 1–4.
10. Walker, H.; Hall, W.; Hurst, J. *Clinical Methods: The History, Physical, and Laboratory Examinations*; Butterworths: Boston, MA, USA, 1990.
11. Shanthi, K.; Santhi, S.; Reddy, S. Others Handy Non-Invasive Blood Glucose Estimator using Arduino and NodeMCU. In Proceedings of the 2023 International Conference on Intelligent Data Communication Technologies and Internet of Things (IDCIoT), Bengaluru, India, 5–7 January 2023; pp. 866–869.
12. Zhu, W.; Yu, H.; Pu, Z.; Jin, C.; Ma, Y.; Zheng, H.; Li, W.; Li, C.; Zhang, X.; Li, D. Accurate Non-Invasive Glucose Monitoring Based on Ph-Calibration. In Proceedings of the 2024 IEEE 37th International Conference On Micro Electro Mechanical Systems (MEMS), Austin, TX, USA, 21–25 January 2024; pp. 379–382.
13. Ribas, R.; Moreira, J.; Uriz, A. A Novel Fingertip Model for Microwave Non-Invasive Blood Glucose Simulations. *IEEE Sen. Lett.* **2024**, *8*, 3500604,
14. Hanna, J.; Costantine, J.; Kanj, R.; Eid, A.; Tawk, Y.; Ramadan, A. Electromagnetic based devices for non-invasive glucose monitoring. In Proceedings of the 2018 IEEE Conference On Antenna Measurements & Applications (CAMA), Västerås, Sweden, 3–6 September 2018; pp. 1–4.
15. Joel, T.; Sakthipriya, R.; Reena, J.; Poojha, A. Novel Approach to Non-Invasive Blood Glucose Monitoring Based on Visible Laser Light. In Proceedings of the 2022 International Conference on Automation, Computing and Renewable Systems (ICACRS), Coimbatore, India, 15–16 October 2018; pp. 54–57.
16. Ghoreishizadeh, S.; Taurino, I.; De Micheli, G.; Carrara, S.; Georgiou, P. A differential electrochemical readout ASIC with heterogeneous integration of bio-nano sensors for amperometric sensing. *IEEE Trans. Biomed. Circuits Syst.* **2017**, *11*, 1148–1159. [CrossRef]
17. Khamsavi, A.; Abdi, Y.; Meymian, M. A novel two-electrode nonenzymatic electrochemical glucose sensor based on vertically aligned carbon nanotube arrays. *IEEE Sens. Lett.* **2019**, *3*, 4500104. [CrossRef]
18. Villena, Gonzales, W.; Mobashsher, A.; Abbosh, A. The progress of glucose monitoring—A review of invasive to minimally and non-invasive techniques, devices and sensors. *Sensors* **2019**, *19*, 800. [CrossRef] [PubMed]
19. Marius, I.; Sever, P. Algorithms of absorbance and colorimeter for measuring blood glucose. In Proceedings of the 2019 11th International Symposium on Advanced Topics in Electrical Engineering (ATEE), Bucharest, Romania, 28–30 March 2019; pp. 1–6.

20. Burrin, J.; Price, C. Measurement of blood glucose. *Ann. Clin. Biochem.* **1985**, *22*, 327–342. [CrossRef]
21. Volsko, T.; Chatburn, R.; El-Khatib, M. *Equipment for Respiratory Care*; Jones & Bartlett Learning: Burlington, MA, USA, 2020.
22. YSI Incorporated. *YSI 2700 SELECT Biochemistry Analyzer User's Manual*; YSI Incorporated: Yellow Springs, OH, USA, 2009.
23. Liang, Y.; W.; Wanderer, J.; Nichols, J.; Klonoff, D.; Rice, M. Blood gas analyzer accuracy of glucose measurements. *Mayo Clin. Proc.* **2017**, *92*, 1030–1041. [CrossRef] [PubMed]
24. Sahu, S.; Chowdhury, D.; Chattopadhyay, M. Design of MEMS capacitive sensor for the identification of cancerous blood cell: A simulation study. In Proceedings of the 2015 International Conference on Smart Sensors and Systems (IC-SSS), Bangalore, India, 21–23 December 2015; pp. 1–4.
25. Guin, S.; Chattopadhyay, M. Advancement and challenges for non-invasive monitoring of blood glucose: A review. In Proceedings of the 2020 International Conference on Advances in Medical Physics and Healthcare Engineering (AMPHE 2020), Kolkata, India, 25–26 September 2020; Springer: Berlin/Heidelberg, Germany, 2020; pp. 101–113.
26. Ullah, A.; Zulfiqar, M.; Khan, M.; Zubair, M.; Mehmood, M.; Massoud, Y. Fast response facile fabricated ide-based ultra-sensitive humidity sensor for medical applications. *ACS Omega* **2023**, *8*, 16842–16850. [CrossRef] [PubMed]
27. Aldhaheri, R.; Kamili, J.; Nella, A.; Sobahi, N. A novel compact highly sensitive non-invasive microwave antenna sensor for blood glucose monitoring. *Open Phys.* **2023**, *21*, 20230107. [CrossRef]
28. Zoric, N.; Iavorschi, A.; Sireteanu, M.; Viziteu, G.; Ciobanu, R. Design and simulations of idc sensor using comsol multyphysics and dielectric spectroscopy of ltcc spectroscopy of ltcc materials materials materials. *Bul. Agir* **2013**, *3*, 63–69.
29. Li, M.; Lv, Y.; Jin, Y.; Li, Y. Simulation Research on Interdigitated Electrodes based sensors in water solution monitoring. *J. Phys. Conf. Ser.* **2022**, *2417*, 012026. [CrossRef]
30. Muaz, A.; Hashim, U.; Liu, W.; Ibrahim, F.; Thong, K.; Mohktar, M. Fabrication of interdigitated electrodes (IDE's) by conventional photolithography technique for pH measurement using micro-gap structure. In Proceedings of the 2014 IEEE Conference on Biomedical Engineering and Sciences (IECBES), Kuala Lumpur, Malaysia, 8–10 December 2014; pp. 146–150.
31. MacKay, S.; Hermansen, P.; Wishart, D.; Chen, J. Simulations of interdigitated electrode interactions with gold nanoparticles for impedance-based biosensing applications. *Sensors* **2015**, *15*, 22192–22208. [CrossRef]
32. Hatada, M.; Loew, N.; Okuda-Shimazaki, J.; Khanwalker, M.; Tsugawa, W.; Mulchandani, A.; Sode, K. Development of an interdigitated electrode-based disposable enzyme sensor strip for glycated albumin measurement. *Molecules* **2021**, *26*, 734. [CrossRef] [PubMed]
33. Nguyen, S.; Vu, P.; Tran, M. Glucose sensors based on chitosan capped Zns doped Mn nanomaterials. *IEEE Sens. Lett.* 2023, *7*, 4500304. [CrossRef]
34. Nguyen, S.; Vu, P.; Nguyen, H.; Tran, M. Optical glucose sensors based on chitosan-capped ZnS-doped Mn nanomaterials. *Sensors* **2023**, *23*, 2841. [CrossRef] [PubMed]
35. Jiang, T.; Ye, X.; Tian, Z.; Shaheen, M.; Khorshed, A.; Feng, Y.; Li, B.; Zhang, Y.; Wang, X.; Chen, J. Sensitivity studies and optimization of an impedance-based biosensor for point-of-care applications. *Biosens. Bioelectron. X* **2024**, *18*, 100479. [CrossRef]
36. Mondol, S.; Mallik, S.; Chattopadhyay, M. ResearchGate Home Page. Available online: https://www.researchgate.net/publication/332834825_MEMS_based_Blood_Cell_Counting_Device (accessed on 1 September 2024).
37. Chattopadhyay, M.; Chowdhury, D.; Sahu, S. Study of dielectric properties of leukocytes for the determination of malignancy by capacitive type MEMS sensor. *Microsyst. Technol.* **2019**, *25*, 1613–1618. [CrossRef]
38. Chattopadhyay, M.; Chowdhury, D. Design and performance analysis of MEMS capacitive pressure sensor array for measurement of heart rate. *Microsyst. Technol.* **2017**, *23*, 4203–4209. [CrossRef]
39. Chowdhury, D.; Chattopadhyay, M. Development of a low-power microcontroller-based wrist-worn device with resource-constrained activity detection algorithm. *IEEE Trans. Instrum. Meas.* **2020**, *69*, 7522–7529. [CrossRef]
40. Mallik, S.; Chowdhury, D.; Chattopadhyay, M. Development of a Power Efficient Hearing Aid Using MEMS Microphone. In Proceedings of the Social Transformation—Digital Way: 52nd Annual Convention of the Computer Society of India, CSI 2017, Kolkata, India, 19–21 January 2018; Revised Selected Papers 52, pp. 369–375.
41. Kumar, V.; Preeti, K.; Saini, V.; Kaushik, A.; Sharma, S. Interdigitated Electrodes (IDEs)-Supported Biosensing for Efficient Point-of-Care Applications. *ECS Sens. Plus* **2024**, *3*, 043401. [CrossRef]
42. Sabiri, I.; Bouyghf, H.; Raihani, A. Optimal interdigitated electrode sensor design for biosensors using differential evolution algorithm. *E3S Web Conf.* **2022**, *351*, 01031. [CrossRef]
43. Li, P.; Boilla, S.; Wang, C.; Lin, P.; Kuo, C.; Tsai, T.; Lee, G. A self-driven, microfluidic, integrated-circuit biosensing chip for detecting four cardiovascular disease biomarkers. *Biosens. Bioelectron.* **2024**, *249*, 115931. [CrossRef] [PubMed]
44. Assaifan, A.; Almansour, R.; Alessa, J.; Alhudaithy, S.; Fakhouri, A.; Alsaleh, A. Roles of Interdigitated Electrode Geometry in Non-Faradaic Impedimetric Biosensors. *J. Electrochem. Soc.* **2024**, *171*, 087515. [CrossRef]
45. Mielewczyk, L.; Galle, L.; Niese, N.; Grothe, J.; Kaskel, S. Precursor-Derived Sensing Interdigitated Electrode Microstructures Based on Platinum and Nano Porous Carbon. *ChemistryOpen* **2024**, *13*, e202400179. [CrossRef] [PubMed]

46. Korek, E.; Teotia, R.; Herbig, D.; Brederlow, R. Electrochemical Impedance Spectroscopy for Ion Sensors with Interdigitated Electrodes: Capacitance Calculations, Equivalent Circuit Models and Design Optimizations. *Biosensors* **2024**, *14*, 241. [CrossRef]
47. Thakur, A.; Srivatava, V.; Park, H.; Kebaili, I.; Boukhris, I.; Joo, Y.; Sung, T.; Kumar, A.; Vaish, R. Calligraphic interdigitated capacitive sensors for green electronics. *Sci. Rep.* **2024**, *14*, 15685. [CrossRef]
48. Habboush, S.; Rojas, S.; Rodríguez, N.; Rivadeneyra, A. The Role of Interdigitated Electrodes in Printed and Flexible Electronics. *Sensors* **2024**, *24*, 2717. [CrossRef] [PubMed]
49. Amers, E.; Orme, B.; Shi, Y.; Torun, H.; Dodd, L. Embroidered Interdigitated Electrodes (IDTs) with Wireless Readout for Continuous Biomarker Monitoring. *Sensors* **2024**, *24*, 4643. [CrossRef]
50. Borchers, J.; Clark, M.; Van Scoy, S.; Anand; R. Array of interdigitated bipolar electrodes for selective capture and analysis of melanoma cells. *ChemElectroChem* **2024**, *11*, e202300345. [CrossRef]
51. Zhang, J.; Luan, Y.; Ma, Q.; Hu, Y.; Ou, R.; Szydzik, C.; Yang, Y.; Trinh, V.; Ha, N.; Zhang, Z.; et al. Large-area grown ultrathin molybdenum oxide for label-free sensitive biomarker detection. *Nanoscale* **2024**, *16*, 13061–13070. [CrossRef]
52. Chowdhury, D.; Chattopadhyay, M. Study and classification of cell bio-impedance signature for identification of malignancy using artificial neural network. *IEEE Trans. Instrum. Meas.* **2021**, *70*, 2505908. [CrossRef]
53. Guin, S.; Chowdhury, D.; Chattopadhyay, M. A capacitive sensor-based approach for type-2 diabetes detection via bio-impedance analysis of erythrocytes. *Sens. Int.* **2024**, *6*, 100300. [CrossRef]
54. Gemanam, S.; Suardi, N.; Ikyo, B.; Oluwafemi, S. Frequency characterization of dielectric parameters and impedance of irradiated diabetic blood using He-Ne laser and non-diabetic human blood samples. *J. Phys. Conf. Ser.* **2021**, *1892*, 012024. [CrossRef]
55. Guin, S.; Chowdhury, D.; Chattopadhyay, M. A novel methodology for detection of Malaria. *Microsyst. Technol.* **2024**, *30*, 1477–1484. [CrossRef]
56. Mortadi, A.; Melouky, A.; Chahid, E.; Moznine, R.; Cherkaoui, O. Studies of the Clausius-Mossotti Factor. *J. Phys. Stud.* **2016**, *20*, 4001-1. [CrossRef]
57. Malleo, D.; Nevill, J.; Lee, L.; Morgan, H. Continuous differential impedance spectroscopy of single cells. *Microfluid. Nanofluidics* **2010**, *9*, 191–198. [CrossRef] [PubMed]
58. Sun, T.; Morgan, H. Single-cell microfluidic impedance cytometry: A review. *Microfluid. Nanofluidics* **2010**, *8*, 423–443. [CrossRef]
59. Kamat, D.; Bagul, D.; Patil, P. Blood glucose measurement using bioimpedance technique. *Adv. Electron.* **2014**, *2014*, 406257. [CrossRef]
60. Desouky, O. Rheological and electrical behavior of erythrocytes in patients with diabetes mellitus. *Rom. J. Biophys.* **2009**, *19*, 239–250.

Disclaimer/Publisher's Note: The statements, opinions and data contained in all publications are solely those of the individual author(s) and contributor(s) and not of MDPI and/or the editor(s). MDPI and/or the editor(s) disclaim responsibility for any injury to people or property resulting from any ideas, methods, instructions or products referred to in the content.